Journal of Materials, Processing and Design (2022)
Clausius Scientific Press, Canada

DOI: 10.23977/jmpd.2022.060203
ISSN 2516-0923 Vol. 6 Num. 2

Study on the Microstructure Characteristics and Mechanical Properties of Dissimilar Weld Joints of Coiled Tubing

Chuan Wang[1,2,a,*]

[1]*State Key Laboratory of Petroleum Resources and Prospecting, China University of Petroleum (Beijing), Beijing, China*
[2]*School of Mechatronic Engineering, Southwest Petroleum University, Chengdu, China*
[a]*cwang0820@163.com*
**Corresponding author*

Keywords: Dissimilar welding, Microstructure, Tensile test, Charpy impact toughness test

Abstract: This work aims to investigate the microstructure and the mechanical behavior of dissimilar API X80-AISI 4130 steel welded joints of coiled tubing. The microstructure at the weld interface of the AISI 4130 steel side results in a relatively lower toughness. The HAZ of AISI 4130 steel has an obvious coarsening phenomenon. The tensile tests show that the deformation process of the dissimilar weld joint is mainly controlled by the two base materials: AISI 4130 steel at the beginning of the deformation and API X80 steel at its end. Charpy impact toughness tests conducted on dissimilar welded specimens led us to conclude that the higher Ni content accounts for a more gradual decline in impact toughness for AISI 4130 steel.

1. Introduction

Coiled tubing (CT) is an important, economical, and safe way for downhole intervention operation during petroleum and natural gas production with high pressure. In recent years, the demand for deep-depth petroleum and natural gas is gradually increased, and the capacity of oil and gas tubing has been developing greatly. API X80 steel and AISI 4130 steel are widely used as structural materials of welded dissimilar joints for downhole wells, with high strength, toughness, weldability, and corrosion resistance, and have been used in the project of natural gas development world while. When coming to practical application, it often involves the welding process of API X80 steel to AISI 4130 steel, and the risk of crack initiation can be expected due to local microstructural heterogeneity. This difference in microstructure can cause the crack initiation near the fusion line, which is a factor that can increase the local stress concentration in the adjacent heat-affected zone as reported in previous works. These cracks can grow under given service conditions causing the fracture of the welded structure [1][2].

Recently, great efforts have been devoted to studying the API X80 steel and the AISI 4130 steel weld joints separately. For the API X80 steel welds, several research works have been carried out to examine the effect of weld metal chemistry and welding defects, the corrosion behavior in aggres-

sive environments, and the effect of heat treatments on their microstructure and mechanical behavior. Lee et al. [3] reported that the local brittle zone (LBZ) of the heat-affected zone (HAZ) of the welded joint of TMCP steels appeared, attributed mainly to the significant increase in the amount of martensite. Rak and Treiber [4] reported that due to a mismatch of weld joints fabricated in HSLA steels, fracture deviation from the coarse-grained heat affected zone (CGHAZ) into weld or base metal occurred. Moreover, the fracture toughness of X80 steel pipeline steel has been studied comprehensively using the Charpy impact toughness test and the drop-weight tear test (DWTT) [5][6][7][8], these impact tests are suited to evaluate fracture toughness of HSLA steel pipelines under dynamic loading conditions. For the AISI 4130 steel as well, the studies of mechanical properties of welding mainly focus on tensile strength, conventional S-N curve fatigue property, and Charpy impact toughness [9]. Guo, et al. [10] note that some variation in fracture mode occurs in that there is a tendency for the fracture to propagate into the base metal rather than weld metal. They indicated that only in a few cases, a true transition temperature as measured by absorbed energy can be obtained. Bull and Vogt studied the influence of heat treatment on the fatigue behavior of AISI 4130 steel [11].

In this study, the TIG welded dissimilar joint of the API X80 steel and AISI 4130 steel are investigated covering the entire range of weld seams. The hardness distribution test, the metallographic observation, the tensile test, and the fracture toughness test are carried out. The metallurgical structures, the basic mechanical properties, and the fracture toughness values of the specimen at different locations of the welded joint are obtained. The variation of the fracture toughness values of the X80 steel weldment is discussed based on the microstructures.

2. Background

A great deal of research has been conducted in recent years to improve the understanding of CT joint life. Joint life prediction models are now being used to predict when a joint will reach the end of its fatigue life. This understanding has improved the reliability of CT service.

The weakest point in a CT joint is at the weld, especially the dissimilar weld joints. CT manufacturers have made significant improvements to the weld seam during fabrication. Instead of performing tube-to-tube or "butt" welds on completed CT tube sections, manufacturers now weld the strips together in sections before they are laminated into tubes. In this type of welding, the ends of the strip are cut at an angle or "bias", so these welds are often referred to as "bias" or "CM" (continuous milled) welds. The beveling allows the weld to be spiraled along the axis of the tube, thereby increasing the axial strength of the weld. This strip welding technique greatly improves the reliability of CT tubes.

In the field, it is often necessary to join two CT sections. the strip welding technique cannot be used, because the CT is already a tube. Therefore, butt welds must be used. These butt welds are the most unreliable part of the CT.

A research project was conducted to better understand CT welds, which involved three main tasks:

- Weld Analysis - A previous project was performed in which nearly 400 CT fatigue tests were performed to better understand the fatigue life of CT welds. Many of the failed samples were provided to this project for analysis.
- Welding procedures - Welding procedures from different sources of CTs were reviewed along with the complete welding process. Recommended procedures were prepared for four different welding situations.
- Alternative Techniques - Ten alternative welding techniques were studied to determine if they could be applied to CT welding.

We found a large number and variety of manual welding procedures currently in use on CTs. While the industry believes that the requirements for all welding procedures are similar, this study found significant variation in the application of the gas tungsten arc welding process. In some cases, the selection of parameters or weld variables considered critical to weld integrity is determined by the welder performing the task.

In this project, five manual welding procedures from CT manufacturers and service companies were reviewed. Many experts were interviewed for their opinions. The autogenous welding procedure is recommended for CTs with thin wall thicknesses. this procedure requires a high level of skill for manual welders and a high helium mixture. The high penetration V-groove welding procedure is recommended for thicker CTs. again, a high skill level and a high helium mixture are required. Low-penetration welding procedures require minimal welder skill to perform and require only argon gas. This is probably the most suitable procedure for use in the field.

3. Experimental procedure

3.1. Material and welding procedure

The chemical compositions of the materials used are presented in Table 1. The dimensional designation of the specimen was 55×10×10 mm. Before welding, all specimen surfaces were ground with an abrasive paper to remove impurities, followed by cleaning with acetone.

TIG welding trials were performed using mechanized equipment in which a welding torch with a 2.5 mm diameter, 1.5% lanthanide tungsten electrode, was traveled at a constant speed. The included angle of the electrode tip was selected at 60 °. The power supply used in TIG welding had a constant-current characteristic. An autogenous, single-pass TIG welding with DCEN polarity was used to make a bead-on-plate weld. The welding current and travel speed were selected to be 220A and 150mm/min, respectively.

Table 1: Chemical composition of API X80 steel and AISI 4130 steel(wt.%)

	API X80 steel	AISI 4130 steel	TIG wire
C	0.06	0.19	0.105
Si	0.16	0.25	0.54
Mn	1.78	1.92	1.14
P	0.013	0.015	0.009
S	0.003	0.002	0.008
Cr	0.03	0.10	0.08
Ni	0.07	0.92	0.80
Mo	0.24	0.31	0.32
Cu	0.08	0.12	0.02
Al	0.02	0.005	0.007
Ti	0.007	0.003	0.005
V	0.036	0.06	0.046
Nb	-	0.09	-
As	-	0.012	-
Fe	Balance	Balance	Balance

3.2. Metallographic preparation and microscopic analysis

After welding, the metallographic specimens were sectioned perpendicular to the longitudinal axis of the weld. All specimens were prepared using standard operating procedures, including mounting, grinding, rough polishing, and fine polishing, followed by etching. The shape of the weld and the microstructures of the weldment were photographed using an optical microscope. The weld

depth (D), bead width (W), and HAZ width of the specimens were measured using a CARL ZEISS microscope. In this study, CARLZEISS's microscope with monocular head, 50×total magnification, and tungsten illumination created a 2-D image for measuring the dimensions of the specimens.

3.3. Mechanical testing

The Vickers microhardness tests were used to evaluate the macroscopic strength of the weldment. The measurements were made in the cross-section of the weld using an instrumented indentation machine microhardness tester (Wilson, 452SVD). For the single weld beads, the indentations were performed along a straight line crossing the weld from top to bottom, and reaching the heat-affected zone (HAZ) of the base metal. The welded specimen was measured in terms of Vickers microhardness under an indentation load of 300g for 15s.

To examine the tensile properties of weldment, tensile test specimens were machined from single-pass bead-on-plate welds. The tensile test specimen had a gauge length of 12.5 mm with a cross-sectional area of 2×5 mm. The testing procedure was performed according to ASTM A370, using a WPM 1000KN tensile test frame, with a strain rate of 1 mm/min.

The Charpy impact toughness test was used to examine the toughness properties of the weldment. V-notch Charpy impact toughness test specimens were extracted from the single-pass weld metal. A Charpy impact specimen was used in this study (55×5×10) mm, the notch was 2 mm through 5 mm depth, with impact tests conducted at temperatures of −20°C. The Charpy impact machine used was a Zwick/Roell RKP450 of 400 J capacity.

4. Results and discussion

4.1. Microstructures

The typical API X80 steel to AISI 4130 steel TIG welded joint and cross-sectional macrograph are shown in Figure 1. The flash formed on the API X80 steel side is larger than that on the AISI 4130 steel side. Different characteristic zones, such as weld interface and heat affected zone (HAZ) on both sides are analyzed in detail on the etched cross-section of the joint.

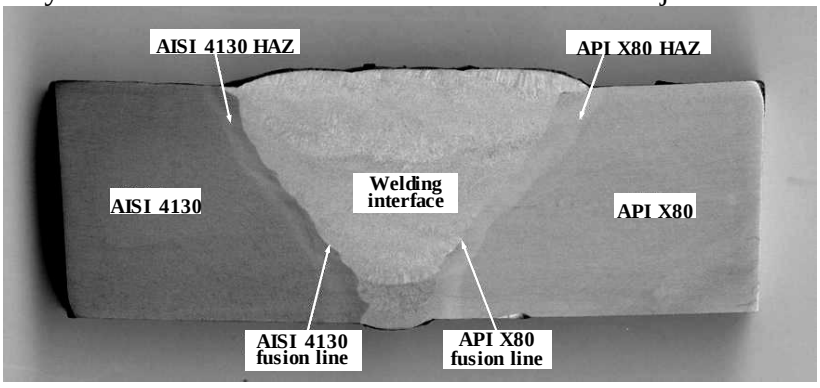

Figure 1: Macrographs of weld joints

The typical microstructures in different zones on AISI 4130 steel side are shown in Figure 2 (a) and (b). The microstructure at the weld interface predominantly contains a pro eutectoid ferrite (PF) interlocking structure with a small fraction of granular bainite (GB) and acicular ferrite (AF), which will result in a relatively lower toughness. The grain size measurement results showed that the weld metal has an average grain size of 1.96μm. The microstructure of HAZ with obvious coarsening phenomenon contained tempered martensite (TM), tempered sorbate (TS), and GB.

The typical microstructures in different zones on the API X80 steel side are shown in Figures 2

(c) and (d). The microstructure at the weld interface varies along the radial direction. The microstructure predominantly contains an AF interlocking structure with a small fraction of GB and Widmanstatten ferrite (WF). The grain size measurement results showed that the weld metal has an average grain size of 2.38μm. The microstructure of HAZ contained AF, sorbate, and GB, and the AF morphologies are slightly higher compared to single-pass welding. However, AF remains the dominant constituent for both weld interfaces.

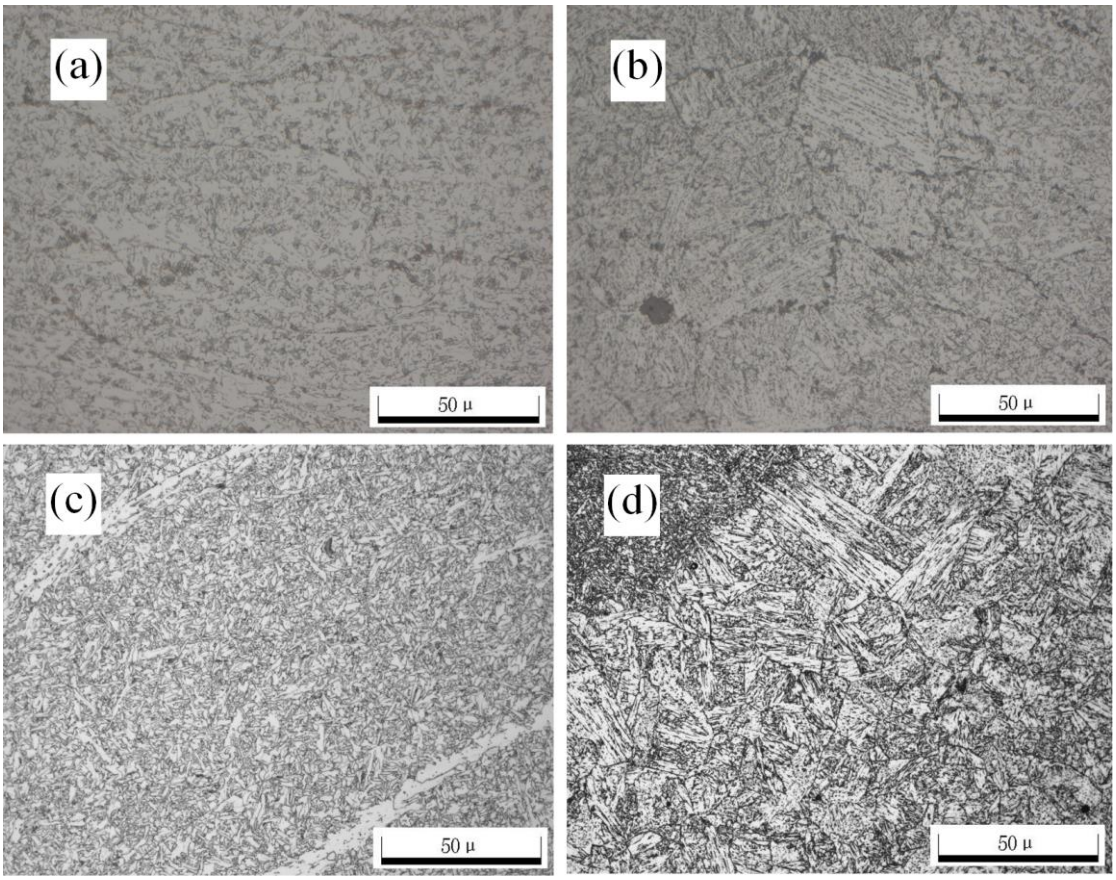

Figure 2: Metallographic photographs of the dissimilar steel weldment: 2(a) Weldment on AISI 4130 steel side, 2(b) HAZ on AISI 4130 steel side, 2(c) Weldment on API X80 steel side, 2(d) HAZ on API X80 steel side

4.2. Hardness distributions

The results of Vickers microhardness tests are shown in Figure 3. The microhardness presents an uneven distribution. The average hardness values of base materials of AISI 4130 steel and API X80 steel are 235HVand 242HV, respectively. Microhardness values of the HAZ depend on the phase constituents and the extent of local recrystallization. The hardness distribution shows a maximum hardness (281HV) at the HAZ of AISI 4130 steel. Then, microhardness falls below the value of base material API X80 steel and then rises slowly with the approach to the base material on the HAZ of API X80 steel while it falls to and keeps at the average level on the API X80 steel side. The sharp variation of hardness in the weld interface is related to the online ring structure and the intercalated microstructure. Even though grains at the nugget zone are recrystallized and are much smaller than the base material, the microhardness rises immediately in other locations. The hardness distribution shows a minimum hardness (229HV) at the base material of the AISI 4130 steel side, which is lower than

that of its HAZ. Meanwhile, the hardness of the weld interface varied in the range of 233-247HV.

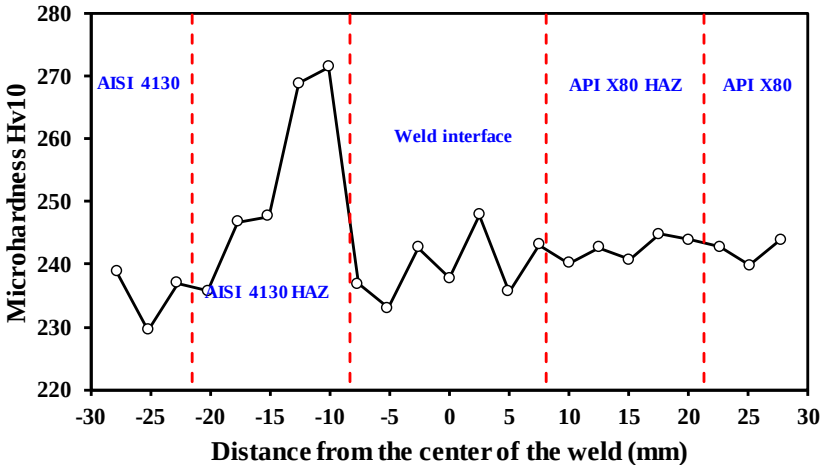

Figure 3: Vickers hardness of dissimilar weld joint

4.3. Tensile and toughness properties

Figure 4 presents the stress-strain curve for the specimen in the as-deposited condition for single-pass weld beads. The average ultimate tensile strength (UTS) and elongation-to-failure (ε_f) at 20°C were 690 MPa and 14.8% respectively. Except for AISI 4130 steel, the specimen with the complete weld joint presents less susceptibility to plastic deformation. This can be explained by both the high yield strength (YS) and the UTS of the HAZ. Information concerning the YS and the UTS of the HAZ, in some cases, can be obtained from hardness measurements. The estimation of tensile properties from hardness measurements has been extensively reported in the literature. Since the hardness level of both HAZs is higher than that of the two BMs, the strengths corresponding to the onset of their plastic deformation may be superior to the ones of the BMs. The deformation process of the dissimilar weld joint is mainly controlled by the two base materials: AISI 4130 steel at the beginning of the deformation and API X80 steel at its end.

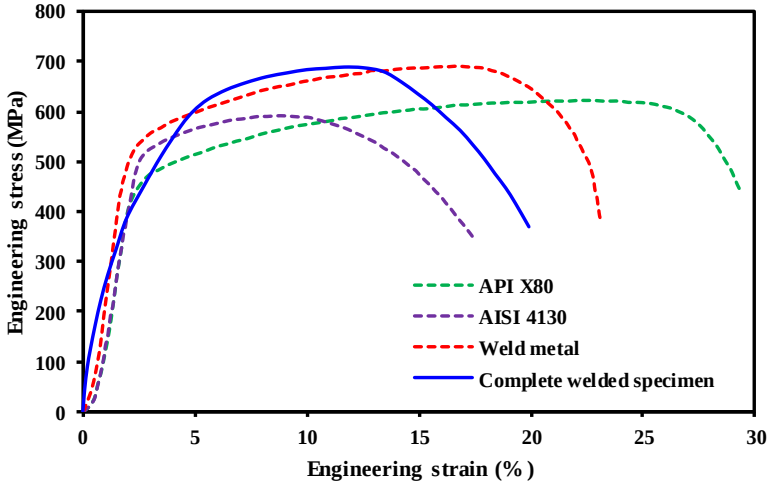

Figure 4: Engineering stress-strain curves obtained from base metal and tensile specimen

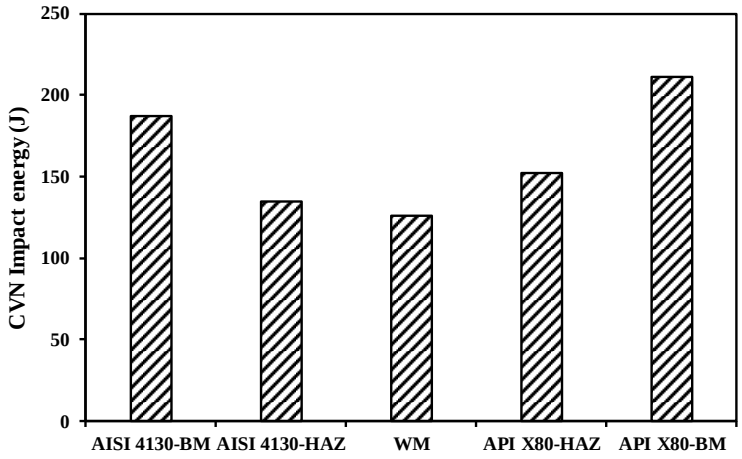

Figure 5: Evolution of the impact energy across the weld joint

The toughness results are presented in Figure 5, where it can be noted that for the testing temperatures of −20℃, API X80 steel is tougher than AISI 4130 steel. The Charpy impact test results indicate that the HAZ of API X80 steel exhibits higher upper shelf impact toughness than that of HAZ of AISI 4130 steel, it is expected that the ductile to brittle transition temperature is below this value. The higher upper shelf values of AISI 4130 steel are in agreement with the lower hardness results observed in this study. From Table 1, it can be seen that AISI 4130 steel has 0.92-wt% Ni compared to 0.07-wt% nickel in API X80 steel. The addition of Ni can flatten the Charpy impact transition curve and increase lower shelf toughness, at the same time that the upper shelf toughness will be decreased for weld metal deposits as the Ni content increases. This behavior was observed in AISI 4130 steel, and justifies due to high Ni content compared to API X80 steel.

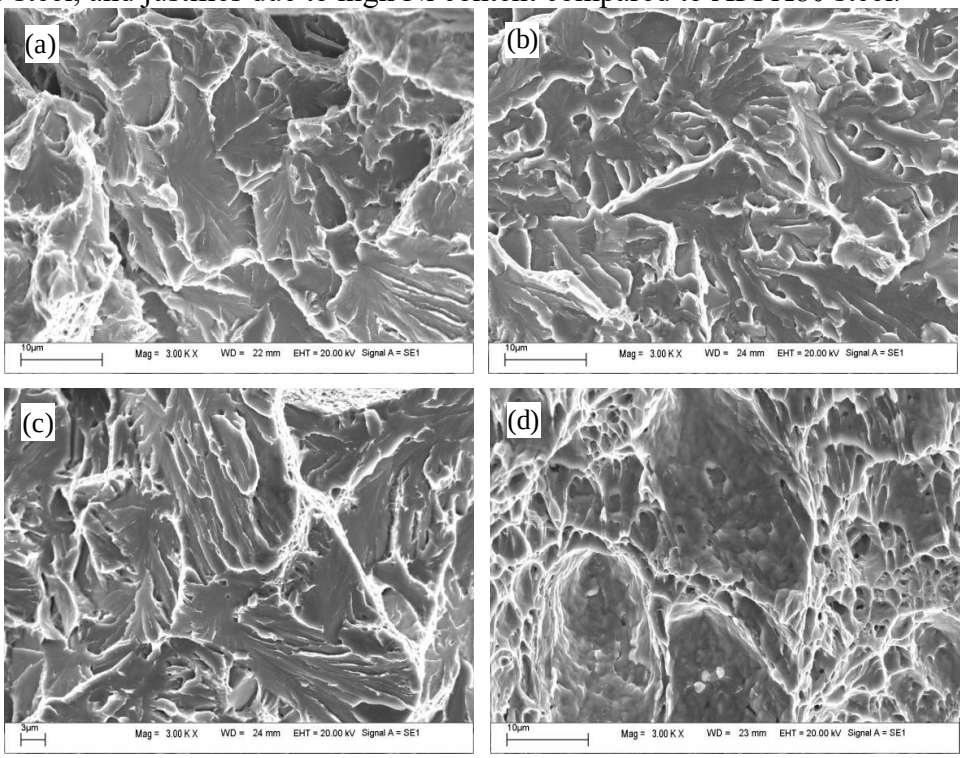

Figure 6: SEM images of Charpy fracture surfaces (at −20℃): 6(a) AISI 4130 steel HAZ, 6(b) AISI 4130 steel fusion line, 6(c) API X80 steel HAZ, 6(d) API X80 steel fusion line

Moreover, increasing the summation of Mo and Ni has the effect of hardening the weld metal and decreasing impact toughness. Since the combination of Ni and Mo for both weld metals are rather different (with values of Ni = 0.92 wt%, and Mo = 0.31 wt% for AISI 4130 steel, versus Ni = 0.07 wt% and Mo = 0.24 wt% for API X80 steel), it appears the reduction in Ni in API X80 steel has helped to avoid a detriment to toughness. One can also note that The Ni content present in AISI 4130 steel accounts for a more gradual decline in impact toughness for AISI 4130 steel.

Further SEM examination of the fracture surfaces was conducted close to the notch area and at the middle area of the fracture surfaces, as shown in Figure 6, and both weld metals presented ductile fracture surfaces characterized by the presence of dimples. The fracture features close to the notch area exhibits an elongated dimple structure, for both weld metal; however, the strain seems to be higher in the case of API X80 steel. When one compares these features, along with the decrease in the hardness and lower carbon equivalent value for API X80 steel, it can explain the higher impact toughness values for this base metal. Most of the inclusions observed in the fracture surface for both weld metals have a size of less than 1μm, which is an ideal size to nucleate GB according to Ref.[12], and thus explains the GB structure shown in Figure 2.

5. Conclusion

The microstructural evolution and the mechanical behavior of an API X80 steel/AISI 4130 steel TIG weld joint have been studied. The main conclusions of this work are summarized as follows:

(1) Dissimilar welding of API X80 steel and AISI 4130 steel results in a microstructural heterogeneity that concerns microstructure, phase constituent, morphology, and phase-volume fractions in the heat-affected zones. The crystalline grains of the AISI 4130 steel HAZ were coarsened at different degrees during the welding process.

(2) The tensile tests conducted on specimens containing the complete weld joint and tensile ones machined from each zone separately led us to conclude that the deformation process of the dissimilar weld joint is mainly controlled by the two base materials: AISI 4130 steel at the beginning of the deformation and API X80 steel one at its end.

(3) Toughness tests put evidence that the higher Ni content present in AISI 4130 steel accounts for the more gradual decline in impact toughness for AISI 4130 steel.

Acknowledgments

The researchers gratefully acknowledge the financial support of the State Key Laboratory of Petroleum Resources and Prospecting Open Subjects (PRP/open-1506), Key Research and Development Project in Key Technical Field of Sichuan Province (2019ZDZX0030), International Science and Technology Innovation Cooperation Program of Sichuan Province (2021YFH0115), and International Science and Technology Cooperation Project of Chengdu (2019-GH02-00039-HZ).

References

[1] Fricke, W. (2003) Fatigue analysis of welded joints: state of development. Mar. Struct., 16(3), 85–200.

[2] Carpinteri, A., et al. (2015) Fracture mechanics based approach to fatigue analysis of welded joints. Eng. Fail. Anal., 49(3), 67–78.

[3] Lee, S., Kim, B.C., Kwon, D. (1992) Correlation of microstructure and fracture properties in weld heat-affected zones of thermomechanically controlled processed steels. Metall. Trans. A, 23A(10), 2803–16.

[4] Rak, I., Treiber, A. (1999) Fracture behaviour of welded joints fabricated in HSLA steels of different strength level. Eng. Fract. Mech., 64(4), 401–15.

[5] Zerbst, U., et al. (2009) Fracture and damage mechanics modelling of thin-walled structures – an overview. Eng.

Fract. Mech., 76(1), 5–43.
[6] Moeinifar, S., Kokabi, A.H., Madaah Hosseini, H.R. (2010) Influence of peak temperature during simulation and real thermal cycles on microstructure and fracture properties of the reheated zones. Mater. Des., 31(6), 2948–55.
[7] Moeinifar, S., Kokab,i A.H., Madaah, H.R. (2011) Effect of tandem submerged arc welding process and parameters of Gleeble simulator thermal cycles on properties of the intercritically reheated heat affected zone. Mater. Des., 32(2), 869–76.
[8] Strnadel, B., Ferfecki, P., Z˘idlík, P. (2013) Statistical characteristics of fracture surfaces in high-strength steel drop weight tear test specimens. Eng. Fract. Mech., 112(5) pp. 1–13.
[9] Emamian, A., Kowkabi, A.H. (2010) Effects of fillerwire composition along with different pre- and post-heat treatment on mechanical properties of AISI 4130 welded by the GTAW process. Mater. Sci. Appl., 1, 135–140.
[10] Guoc W., et al. (2015) Microstructure and mechanical characteristics of a laser welded joint in SA508 nuclear pressure vessel steel. Materials Science and Engineering: A, 625, 65-80.
[11] Bultel, H., Vogt, J. (2010) Influence of heat treatment on fatigue behaviour of 4130 AISI steel. Procedia Engineering, 2(3), 917-924.
[12] Cvetković R.P., et al. (2006) The influence of the oxygen equivalent in a gas-mixture on the structure and toughness of microalloyed steel weldments, J.Serb.Chem.Soc., 71(3), 313-321.